# Direct Laser Writing of Air-Stable p–n Junctions in Graphene

**Byung Hwa Seo, Jongmin Youn, and Moonsub Shim***

Department of Materials Science and Engineering, University of Illinois, Urbana, Illinois 61801, United States

**ABSTRACT** Photo-oxidation of spin-cast films of 6,13-bis-(triisopropylsilylethynyl) pentacene has been exploited to develop a novel means of spatially modulating doping in graphene. The degree of n-doping of initially p-type graphene can be varied by laser irradiation time or intensity with carrier density change up to $\sim 7 \times 10^{12}$ cm$^{-2}$. This n-doping approach is demonstrated as an effective means of creating p–n junctions in graphene. The ability to direct-write arbitrary shapes and patterns of n-doped regions in graphene simply by scanning a laser source should facilitate the exploitation of p–n junctions for a variety of electronic and optoelectronic device applications.

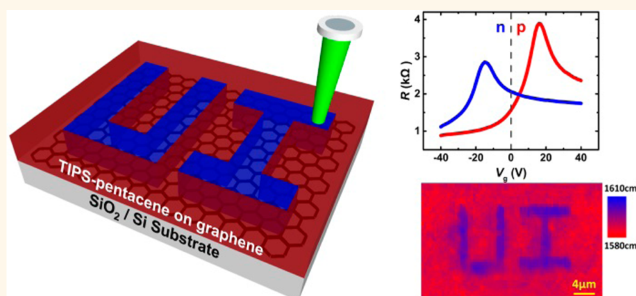


**KEYWORDS:** CVD graphene · TIPS-pentacene · n-type doping · direct laser writing · p–n junction · photocurrent

Graphene, a two-dimensional (2D) sp$^2$ carbon material with exceptional electrical, chemical, optical, and mechanical properties, has emerged as an attractive platform to explore fundamental physics as well as to develop a variety of next-generation devices.[1–6] However, one of the biggest drawbacks of graphene especially for electronics is its zero band gap.[7,8] An alternative means of controlling current flow in graphene is by modulating carrier transmission probability with p–n junctions.[9–11] 2D electron Veselago lensing,[12] in addition to various bipolar electronic[10] and optoelectronic[13–17] devices and complementary circuitry, can be realized with the ability to dope graphene into p- and n-type regions. There is, of course, the important underlying physics such as chiral tunneling[9–11] currently being explored that enables these capabilities. Hence, p–n junctions or, more generally, spatial control over doping profiles is of both fundamental and practical importance.

Broadly speaking, previous efforts to understand and control charge carrier type and/or density in graphene have involved (1) lithographically defined local gates,[10–13,18,19] (2) manipulation of charge interactions with the substrate[14,17,20–24] and/or surrounding atoms/molecules/nanoparticles,[25–32] (3) impurity atom incorporation into the lattice,[15,33] and (4) ferroelectric polarization.[34–36] While some of these approaches allow n-doping of initially p-type graphene in air, there are often drawbacks. Local gates require cumbersome fabrication steps and external voltage and therefore additional power consumption to create differently doped regions.[10–13,18,19] Charge transfer doping from alkali metal[26] or adsorbed molecules[30] are usually achievable only in inert atmosphere or vacuum in addition to requiring lithography to spatially limit regions being doped. Whether it is electrical means[21] or light-induced,[17,23,24] local charging of the substrate can create differently doped regions but eventual charge dissipation, which can often be accelerated by applied gate field (*i.e.*, device operation), can lead to loss of doping. An air-stable means of doping graphene that is also easy to modulate spatially in arbitrary patterns would be highly desirable. Exploiting byproducts of electron beam patterning of hydrogen silsesquioxide to control doping is a significant step along this direction providing high spatial resolution but there are limitations including disorder due to the covalent nature of this process and difficulties in large area patterning.[31,32] Here, we report a new simple approach to spatially modulate doping in graphene by direct laser writing. Photoinduced oxidation of 6,13-bis(triisopropylsilylethynyl) pentacene

* Address correspondence to mshim@illinois.edu.

Received for review July 1, 2014 and accepted July 30, 2014.

**Published online July 30, 2014**
10.1021/nn503574p

© 2014 American Chemical Society

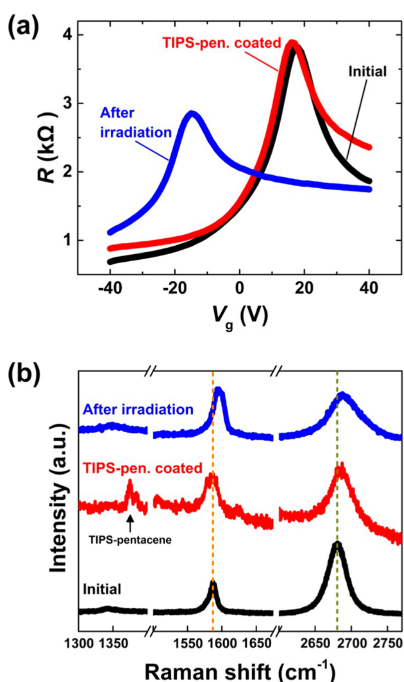


**Figure 1. (a) Resistance *vs* gate voltage ($R-V_g$) curves for a graphene FET as fabricated (black line), after spin coating TIPS-pentacene (red line), and after laser irradiation of the entire channel area (blue line). (b) Raman spectra of graphene before (black line) and after coating with TIPS-pentacene (red line), and after laser irradiation (blue line). The Raman band around ~1375 $cm^{-1}$ (middle spectrum) corresponds to the aromatic C−C stretching mode of TIPS-pentacene, which disappears upon photo-oxidation. Spectra are offset for clarity.**

(TIPS-pentacene) spin-cast on top of graphene causes charge transfer resulting in air-stable n-doping. Direct writing allows arbitrary shapes of n-type regions to be created. The p−n junctions are achieved simply by scanning the laser over half of the channel of graphene field-effect transistors (FETs).

## RESULTS AND DISCUSSION

As-fabricated graphene FETs on $SiO_2$ substrates show p-type behavior with the Dirac point (charge neutrality point) appearing at positive gate voltages ($V_g$), as commonly observed.[30,36−39] The device shown in Figure 1a exhibits the Dirac point at $V_g = +18$ V. The Raman G and 2D peaks shown in Figure 1b are at 1587 and 2681 $cm^{-1}$, respectively, and the ratio of maximum intensities of these two peaks, $I_{2D}/I_G$, is 2.4, comparable to previous reports.[40−43] Spin-coating TIPS-pentacene does not alter the graphene FET characteristics significantly (Figure 1a). The p-type behavior is maintained with only a very slight negative shift of the Dirac point to $V_g = +16$ V. The fact that the conductance does not change noticeably also indicates that the TIPS-pentacene thin film on top of graphene does not contribute significantly to the measured current. TIPS-pentacene-only FET with the same device dimensions exhibits very low current at a very large drain voltage corresponding to ~$2 \times 10^9$ Ω ON-state resistance, which is 6 orders of magnitude larger than the highest resistance state for graphene at the Dirac point (see Supporting Information, Figure S1). A very small downshift and upshift of G and 2D bands, respectively, and a slight broadening of both Raman peaks may be indicative of $\pi-\pi$ interaction with TIPS-pentacene (Figure 1b). Upon laser irradiation of the entire graphene channel, much more significant changes can be seen in both the electrical characteristics and the Raman spectrum. Graphene now becomes n-type with the Dirac point shifting from $V_g = +16$ V to $V_g = -16$ V, corresponding to a carrier density change of ~$6.7 \times 10^{12}$ $cm^{-2}$. Note that the laser irradiation makes TIPS-pentacene-only FET even more electrically insulating with an ON-state resistance of ~$10^{11}$ Ω (Supporting Information, Figure S1). While we observe a net upshift of ~12 $cm^{-1}$ in the G-band upon laser irradiation in Figure 1b, the shift is gradual with an initial downshift which suggests an opportunity to tune the doping level as shown and discussed below. No significant changes in the Raman spectrum is observed when graphene is irradiated under the same condition in the absence of TIPS-pentacene (see Supporting Information Figure S2).

Figure 2a shows the time evolution of Raman G and 2D band frequencies during laser irradiation of TIPS-pentancene coated graphene. On the basis of now well-established Fermi level position dependent electron−phonon coupling,[22,42,44−46] a downshift followed by an upshift in the G-band is expected when graphene is converted from p-type to intrinsic then to n-type. This effect of phonon softening near the Dirac Point is indeed what we observe as TIPS-pentacene above the graphene is photo-oxidized. The inset of Figure 2a shows the corresponding 2D/G peak intensity ratio. The maximum intensity ratio appears at G-band frequency minimum corresponding to charge neutrality point when the graphene becomes intrinsic. These gradual changes in the Raman spectrum indicate that the degree of doping may be controlled by the duration of laser exposure and/or intensity. This is indeed the case as demonstrated in Figure 2b where the Dirac point gradually shifts to more negative gate voltages (becomes more n-type) with increasing laser exposure time (see Supporting Information Figure S3 for the effects of different laser intensities). Changing the laser intensity alters the doping rate and the combination of laser intensity and exposure time may be used to fine-tune doping levels in graphene.

Since our approach to tunable doping only requires spin coating of TIPS-pentacene and a moderate intensity visible light exposure, it can be readily exploited as a simple means of spatially modulating doping. It may be developed into a large area patterning technique using photomasks or, as demonstrated in Figure 3, a versatile direct writing technique. Direct laser writing

of n-doped regions is schematically illustrated in Figure 3a. As a simple example, the letters "UI" have been written and can be easily seen in the optical microscope (Figure 3b). As TIPS-pentacene is irradiated, it becomes transparent in the visible spectral region due to oxidation (as discussed later and as indicated by the disappearance of the TIPS-pentacene aromatic C–C stretch Raman mode in Figure 1b) and an obvious color change occurs in the laser exposed region. The change in doping in the exposed region is verified by the Raman G-band frequency image in Figure 3c which corresponds directly to the optical image. We note that the widths of the laser-induced patterns of TIPS-pentacene on graphene are always slightly wider than patterns made on TIPS-pentacene without graphene. This observation may indicate that graphene can enhance photo-oxidation of TIPS-pentacene and further studies along this direction might provide useful insights on and a new means of exploiting photocatalytic properties of graphene.

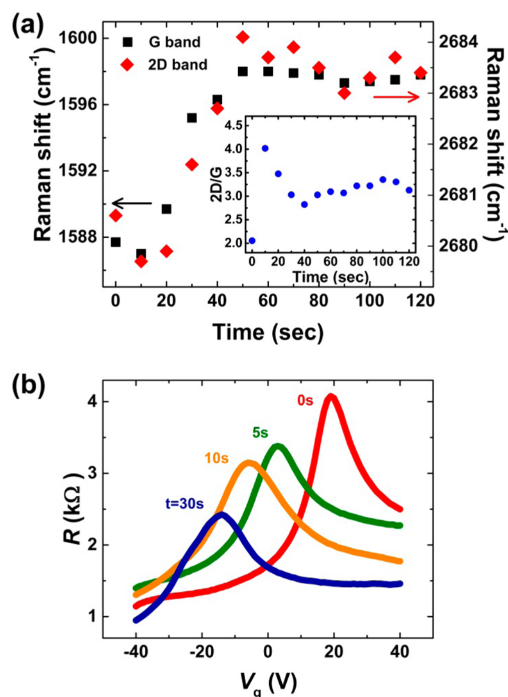


**Figure 2. (a) Spectral positions of G and 2D Raman peaks and the intensity ratio of 2D to G peaks (inset) of graphene coated with TIPS-pentacene on $SiO_2$/Si substrate as a function of time of laser irradiation (laser power = 8.7 mW). (b) Resistance *vs* gate voltage ($R-V_g$) curves for TIPS-pentacene coated graphene FETs after scanning the entire channel with laser (power = 4.1 mW). The irradiation time, *t*, corresponds to the duration at each step including time exposed from previous laser scan (*e.g.*, *t* = 10 s corresponds to the first scan with 5 s exposure time per spot plus a second scan with another 5 s exposure time).**

To establish functionality of devices derived from our spatially resolved doping approach, we now discuss direct writing of p–n junctions. Since as-prepared graphene FETs exhibit p-type behavior, which is maintained upon TIPS-pentacene deposition, p–n junctions can be easily fabricated simply by scanning the laser over half of the graphene channel. The inset of Figure 4a shows the Raman G-band frequency images of the initial p-type graphene with TIPS-pentacene and the same region after irradiation of half the channel. The difference in G-band frequencies between the two differently doped regions is clearly seen. The main panel of Figure 4a shows the changes in the gate dependent resistance of a graphene FET upon p–n junction formation. The initial Dirac point of the p-type graphene near $V_g$ = +20 V splits into two with one

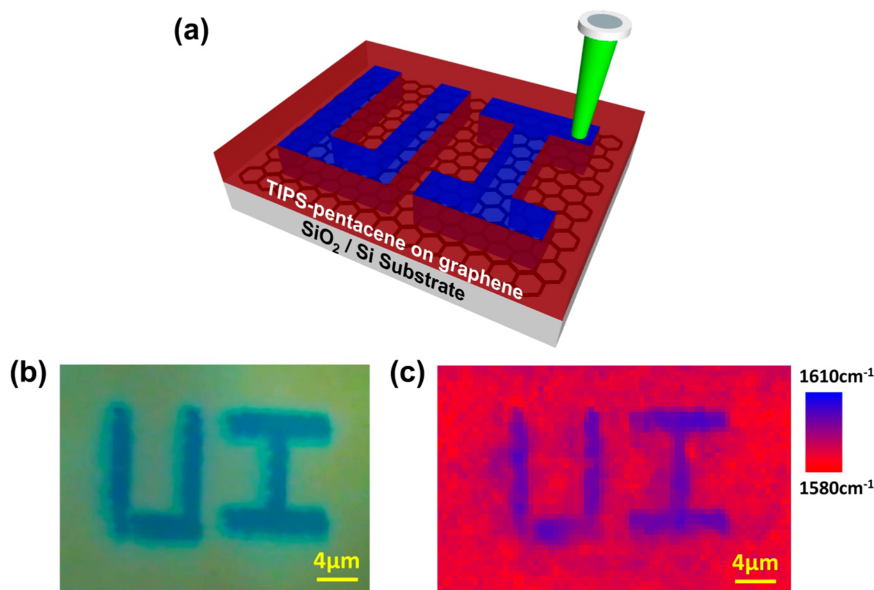


**Figure 3. Direct laser writing of n-doped regions in graphene. (a) Schematic illustration of writing n-doped regions in the form of the letters "UI." (b) Optical image of patterned graphene covered with TIPS-pentacene film. (c) Raman G-band frequency image of the same region of the patterned graphene.**

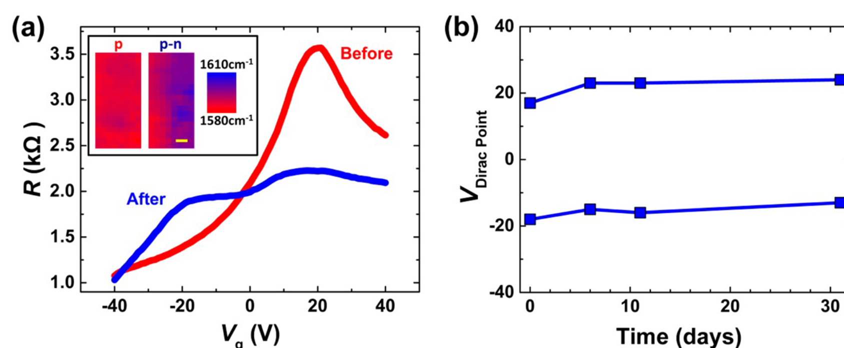


Figure 4. (a) Resistance *vs* gate voltage ($R-V_g$) curves for TIPS-pentacene coated graphene FETs before and after irradiation of half the channel to create p−n junction. Inset shows Raman G-peak frequency images of the graphene FET, p-type after coating TIPS-pentacene, and p−n junction after irradiation of half the channel (scale bar = 1 $\mu$m). (b) The two Dirac point voltages of the graphene p−n junction left out in air over time, demonstrating stability.

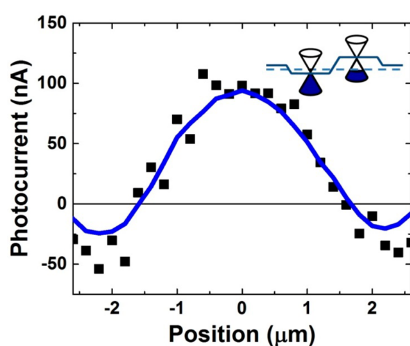


Figure 5. Photoresponse of graphene p−n junction created by partial irradiation of a TIPS-pentacene coated graphene FET. Inset is a schematic band diagram of p−n junction of graphene channel based on the experimental observations.

remaining at similar positive $V_g$ and the second one emerging at $V_g = -18$ V to reflect the n-type region. These dual Dirac points are expected of graphene p−n junctions.[14,15,17,21] Figure 4b shows that the p−n junctions formed are stable in air at least over 30 days with only very slight changes in the positions of the Dirac points.

Figure 5 shows the photoresponse of a graphene p−n junction prepared by our direct laser writing approach. For the photocurrent measurements, a 532 nm laser focused down to ∼1 $\mu$m spot size with power less than 1 mW was used to prevent photodegradation of TIPS-pentacene and scanned from one metal contact across the p−n junction to the other contact. Due to the potential drop near the contacts, a small negative photocurrent is observed near the contacts but the main photocurrent arises at the p−n junction near the center of the channel. The maximum photocurrent of ∼100 nA corresponds to a responsivity of ∼0.1 mA/W, which is smaller than p−n junctions in mechanically exfoliated graphene[13,47−50] but represents one of the largest values for CVD graphene.[15,51]

Finally, to gain insights on the mechanism of n-doping of graphene *via* photo-oxidation of TIPS-pentacene, UV−vis and Fourier transform infrared (FTIR) spectra were examined. As-coated TIPS-pentacene films on quartz substrates exhibit the expected UV−vis absorption spectrum[52] and the presence of graphene does not alter the spectrum as shown in Figure 6a. Laser irradiation leads to photo-oxidation causing a uniform decrease in the optical density. In the mid-IR region, a band at ∼1730 cm$^{-1}$ arising from C═O stretching mode is observed upon laser irradiation consistent with photo-oxidation of TIPS-pentacene. Concurrently, the C≡C stretching mode at ∼2130 cm$^{-1}$ begins to disappear as shown in Figure 6b.[53] A complete loss of TIPS-pentacene aromatic C−C stretch in the Raman spectrum is seen at higher laser intensities as shown in Figure 1b. The two main mechanisms of photo-oxidation of pentacene and its derivatives including TIPS-pentacene are (1) an intersystem crossing in the photoexcited pentacene followed by energy transfer to generate singlet $O_2$, which in turn oxidizes acenes *via* endoperoxides, and (2) electron transfer to generate radical cations of the acenes and $O_2$ anions which can also react to form endoperoxides.[52,54] In the presence of graphene, some of the energy or electron transfer processes from TIPS-pentacene may be to graphene. Energy transfer from photoexcited TIPS-pentacene to graphene followed by a reaction with singlet $O_2$ will lead to p-doping of graphene and therefore an unlikely mechanism for our system. Then, the possible mechanisms based on the two photo-oxidation routes of TIPS-pentacene are (1) electron transfer from the photoexcited TIPS-pentacene to graphene and (2) reaction of graphene with $O_2$ anion. Both of these processes would lead to excess electron density in graphene resulting in net n-type doping. However, the latter case is likely to result in disorder, but as shown in Figure 1b, no significant change in the D-band is observed. Further studies are necessary to elucidate doping mechanism including the identity of possible counterions that would balance charge. We note that this enhanced photo-oxidation of TIPS-pentacene on graphene is an important aspect to consider in integrating graphene

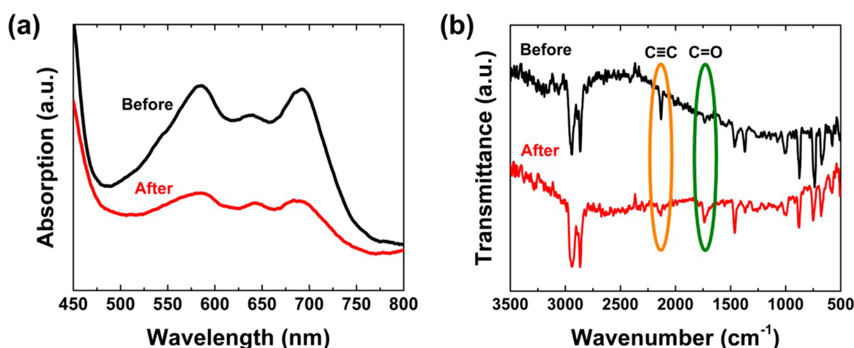


**Figure 6. (a) UV−vis spectrum of TIPS-pentacene spin-coated on graphene on a quartz substrate before (black line) and after (red line) laser irradiation (laser power = 50 mW, spot size = 320 $\mu$m, and irradiation time = 8 h). (b) FTIR spectrum before (black line) and after (red line) laser irradiation of TIPS-pentacene on a KBr substrate. The laser exposure conditions are the same as in (a). Due to the necessity of exposing substrates to water for transferring graphene, graphene was not included for FTIR measurements. FTIR spectra are offset for clarity.**

with organic electronics/optoelectronics as well as in developing graphene-based photocatalysts.

## CONCLUSION

In summary, we have demonstrated a direct writing approach to control doping levels in graphene. Starting from as-synthesized p-type, a carrier density change up to $\sim$6.7 $\times$ $10^{12}$ $cm^{-2}$ has been achieved simply by laser irradiation of TIPS-pentacene spin-cast on graphene. By adjusting the irradiation time (or intensity), we can vary the degree of doping. The functionality and the quality of devices achieved through our approach have been exemplified by the high photocurrent responsivity of the CVD graphene p−n junction. With the ability to direct-write arbitrary shapes and patterns, our approach to air-stable n-doping may provide easily accessible routes to a variety of novel electronic and optoelectronic applications of graphene.

## METHODS

Back-gated graphene FETs were fabricated using single-layer graphene synthesized by chemical vapor deposition (CVD graphene).[36,40] CVD graphene was transferred onto heavily p-doped Si substrates with 100 nm thick $SiO_2$ using established methods.[36,38] Graphene channels were defined using photolithography followed by $O_2$ ion etching. Source and drain electrodes (3 nm Ti/30 nm Pd) were deposited by electron-beam evaporation after photolithography leading to graphene FETs with 5 and 10 $\mu$m channel length and width, respectively. TIPS-pentacene films were deposited by spin-casting a 16 mM solution in chloroform onto graphene FETs at 1000 rpm for 40 s. Unless otherwise noted, laser irradiation was carried out with a 532 nm *cw* diode laser with power = 8.7 mW for 2 min with the beam focused down to $\sim$1 $\mu$m spot size using a 100× air objective under air ambient conditions. Samples were placed on a motorized stage for pattern-writing. For Raman measurements, laser power was kept below 1 mW using a 100× air objective. At this low laser power, no detectable photo-oxidation effects were seen. All measurements were carried out in air at room temperature.

*Conflict of Interest:* The authors declare no competing financial interest.

*Acknowledgment.* This work was supported in part by the National Science Foundation and the Nanoelectronics Research Initiative under Grants DMR-1124696. Experiments were carried out in part in the Frederick Seitz Materials Research Laboratory Central Research Facilities, University of Illinois.

*Supporting Information Available:* Transfer characteristics of a TIPS-pentacene-only FET before and after the laser irradiation, Raman spectra of graphene without TIPS-pentacene at different laser irradiation times, and the evolution of Raman G and 2D peak frequencies of graphene coated with TIPS-pentacene at different laser intensities. This material is available free of charge *via* the Internet at http://pubs.acs.org.

## REFERENCES AND NOTES

1. Novoselov, K. S.; Geim, A. K.; Morozov, S. V.; Jiang, D.; Zhang, Y.; Dubonos, S. V.; Grigorieva, I. V.; Firsov, A. A. Electric Field Effect in Atomically Thin Carbon Films. *Science* **2004**, *306*, 666–669.
2. Zhang, Y.; Tan, Y.-W.; Stormer, H. L.; Kim, P. Experimental Observation of the Quantum Hall Effect and Berry's Phase in Graphene. *Nature* **2005**, *438*, 201–204.
3. Chen, C.; Rosenblatt, S.; Bolotin, K. I.; Kalb, W.; Kim, P.; Kymissis, I.; Stormer, H. L.; Heinz, T. F.; Hone, J. Performance of Monolayer Graphene Nanomechanical Resonators with Electrical Readout. *Nat. Nanotechnol.* **2009**, *4*, 861–867.
4. Avouris, P. Graphene: Electronic and Photonic Properties and Devices. *Nano Lett.* **2010**, *10*, 4285–4294.
5. Schwierz, F. Graphene Transistors. *Nat. Nanotechnol.* **2010**, *5*, 487–496.
6. Polat, E. O.; Kocabas, C. Broadband Optical Modulators Based on Graphene Supercapacitors. *Nano Lett.* **2013**, *13*, 5851–5857.
7. Ohta, T.; Bostwick, A.; Seyller, T.; Horn, K.; Rotenberg, E. Controlling the Electronic Structure of Bilayer Graphene. *Science* **2006**, *313*, 951–954.
8. Castro Neto, A. H.; Guinea, F.; Peres, N. M. R.; Novoselov, K. S.; Geim, A. K. The Electronic Properties of Graphene. *Rev. Mod. Phys.* **2009**, *81*, 109–162.
9. Katsnelson, M. I.; Novoselov, K. S.; Geim, A. K. Chiral Tunnelling and the Klein Paradox in Graphene. *Nat. Phys.* **2006**, *2*, 620–625.
10. Williams, J. R.; DiCarlo, L.; Marcus, C. M. Quantum Hall Effect in a Gate-Controlled p-n Junction of Graphene. *Science* **2007**, *317*, 638–641.
11. Young, A. F.; Kim, P. Quantum Interference and Klein Tunnelling in Graphene Heterojunctions. *Nat. Phys.* **2009**, *5*, 222–226.
12. Cheianov, V. V.; Fal'ko, V.; Altshuler, B. L. The Focusing of Electron Flow and a Veselago Lens in Graphene p-n Junctions. *Science* **2007**, *315*, 1252–1255.
13. Gabor, N. M.; Song, J. C. W.; Ma, Q.; Nair, N. L.; Taychatanapat, T.; Watanabe, K.; Taniguchi, T.; Levitov, L. S.; Jarillo-Herrero,

P. Hot Carrier-Assisted Intrinsic Photoresponse in Graphene. *Science* **2011**, *334*, 648–652.
14. Rao, G.; Freitag, M.; Chiu, H.-Y.; Sundaram, R. S.; Avouris, P. Raman and Photocurrent Imaging of Electrical Stress-Induced p-n Junctions in Graphene. *ACS Nano* **2011**, *5*, 5848–5854.
15. Yan, K.; Wu, D.; Peng, H.; Jin, L.; Fu, Q.; Bao, X.; Liu, Z. Modulation-Doped Growth of Mosaic Graphene with Single-Crystalline p-n Junctions for Efficient Photocurrent Generation. *Nat. Commun.* **2012**, *3*, 1280.
16. Freitag, M.; Low, T.; Xia, F.; Avouris, P. Photoconductivity of Biased Graphene. *Nat. Photonics* **2013**, *7*, 53–59.
17. Kim, Y. D.; Bae, M.-H.; Seo, J.-T.; Kim, Y. S.; Kim, H.; Lee, J. H.; Ahn, J. R.; Lee, S. W.; Chun, S.-H.; Park, Y. D. Focused-Laser-Enabled p-n Junctions in Graphene Field-Effect Transistors. *ACS Nano* **2013**, *7*, 5850–5857.
18. Kim, S.; Nah, J.; Jo, I.; Shahrjerdi, D.; Colombo, L.; Yao, Z.; Tutuc, E.; Banerjee, S. K. Realization of a High Mobility Dual-Gated Graphene Field-Effect Transistor with $Al_2O_3$ Dielectric. *Appl. Phys. Lett.* **2009**, *94*, 062107.
19. Low, T.; Appenzeller, J. Electronic Transport Properties of a Tilted Graphene p-n Junction. *Phys. Rev. B* **2009**, *80*, 155406.
20. Ryu, S.; Liu, L.; Berciaud, S.; Yu, Y.-J.; Liu, H.; Kim, P.; Flynn, G. W.; Brus, L. E. Atmospheric Oxygen Binding and Hole Doping in Deformed Graphene on a $SiO_2$ Substrate. *Nano Lett.* **2010**, *10*, 4944–4951.
21. Chiu, H.-Y.; Perebeinos, V.; Lin, Y.-M.; Avouris, P. Controllable p-n Junction Formation in Monolayer Graphene Using Electrostatic Substrate Engineering. *Nano Lett.* **2010**, *10*, 4634–4639.
22. Nguyen, K. T.; Abdula, D.; Tsai, C.-L.; Shim, M. Temperature and Gate Voltage Dependent Raman Spectra of Single-Layer Graphene. *ACS Nano* **2011**, *5*, 5273–5279.
23. Luo, Z.; Pinto, N. J.; Davila, Y.; Johnson, A. T. C. Controlled Doping of Graphene Using Ultraviolet Irradiation. *Appl. Phys. Lett.* **2012**, *100*, 253108.
24. Ju, L.; Velasco, J.; Huang, E.; Kahn, S.; Nosiglia, C.; Tsai, H.-Z.; Yang, W.; Taniguchi, T.; Watanabe, K.; Zhang, Y.; *et al.* Photoinduced Doping in Heterostructures of Graphene and Boron Nitride. *Nat. Nanotechnol.* **2014**, *9*, 348–352.
25. Schedin, F.; Geim, A. K.; Morozov, S. V.; Hill, E. W.; Blake, P.; Katsnelson, M. I.; Novoselov, K. S. Detection of Individual Gas Molecules Adsorbed on Graphene. *Nat. Mater.* **2007**, *6*, 652–655.
26. Chen, J.-H.; Jang, C.; Adam, S.; Fuhrer, M. S.; Williams, E. D.; Ishigami, M. Charged-Impurity Scattering in Graphene. *Nat. Phys.* **2008**, *4*, 377–381.
27. Dong, X.; Fu, D.; Fang, W.; Shi, Y.; Chen, P.; Li, L.-J. Doping Single-Layer Graphene with Aromatic Molecules. *Small* **2009**, *5*, 1422–1426.
28. Huh, S.; Park, J.; Kim, K. S.; Hong, B. H.; Kim, S. B. Selective N-Type Doping of Graphene by Photo-Patterned Gold Nanoparticles. *ACS Nano* **2011**, *5*, 3639–3644.
29. Liu, Z.; Bol, A. A.; Haensch, W. Large-Scale Graphene Transistors with Enhanced Performance and Reliability Based on Interface Engineering by Phenylsilane Self-Assembled Monolayers. *Nano Lett.* **2011**, *11*, 523–528.
30. Wei, P.; Liu, N.; Lee, H. R.; Adijanto, E.; Ci, L.; Naab, B. D.; Zhong, J. Q.; Park, J.; Chen, W.; Cui, Y.; *et al.* Tuning the Dirac Point in CVD-Grown Graphene through Solution Processed N-Type Doping with 2-(2-Methoxyphenyl)-1,3-dimethyl-2,3-dihydro-1*H*-benzoimidazole. *Nano Lett.* **2013**, *13*, 1890–1897.
31. Ryu, S.; Han, M. Y.; Maultzsch, J.; Heinz, T. F.; Kim, P.; Steigerwald, M. L.; Brus, L. E. Reversible Basal Plane Hydrogenation of Graphene. *Nano Lett.* **2008**, *8*, 4597–4602.
32. Brenner, K.; Murali, R. Single Step, Complementary Doping of Graphene. *Appl. Phys. Lett.* **2010**, *96*, 063104.
33. Usachov, D.; Vilkov, O.; Grüneis, A.; Haberer, D.; Fedorov, A.; Adamchuk, V. K.; Preobrajenski, A. B.; Dudin, P.; Barinov, A.; Oehzelt, M.; *et al.* Nitrogen-Doped Graphene: Efficient Growth, Structure, and Electronic Properties. *Nano Lett.* **2011**, *11*, 5401–5407.
34. Zheng, Y.; Ni, G.-X.; Toh, C.-T.; Zeng, M.-G.; Chen, S.-T.; Yao, K.; Özyilmaz, B. Gate-Controlled Nonvolatile Graphene-Ferroelectric Memory. *Appl. Phys. Lett.* **2009**, *94*, 163505.
35. Hong, X.; Hoffman, J.; Posadas, A.; Zou, K.; Ahn, C. H.; Zhu, J. Unusual Resistance Hysteresis in N-Layer Graphene Field Effect Transistors Fabricated on Ferroelectric $Pb(Zr_{0.2}Ti_{0.8})O_3$. *Appl. Phys. Lett.* **2010**, *97*, 033114.
36. Baeumer, C.; Rogers, S. P.; Xu, R.; Martin, L. W.; Shim, M. Tunable Carrier Type and Density in Graphene/$PbZr_{0.2}Ti_{0.8}O_3$ Hybrid Structures through Ferroelectric Switching. *Nano Lett.* **2013**, *13*, 1693–1698.
37. Levesque, P. L.; Sabri, S. S.; Aguirre, C. M.; Guillemette, J.; Siaj, M.; Desjardins, P.; Szkopek, T.; Martel, R. Probing Charge Transfer at Surfaces Using Graphene Transistors. *Nano Lett.* **2011**, *11*, 132–137.
38. Lee, Y.; Bae, S.; Jang, H.; Jang, S.; Zhu, S.-E.; Sim, S. H.; Song, Y. I.; Hong, B. H.; Ahn, J.-H. Wafer-Scale Synthesis and Transfer of Graphene Films. *Nano Lett.* **2010**, *10*, 490–493.
39. Suk, J. W.; Lee, W. H.; Lee, J.; Chou, H.; Piner, R. D.; Hao, Y.; Akinwande, D.; Ruoff, R. S. Enhancement of the Electrical Properties of Graphene Grown by Chemical Vapor Deposition *via* Controlling the Effects of Polymer Residue. *Nano Lett.* **2013**, *13*, 1462–1467.
40. Li, X.; Cai, W.; An, J.; Kim, S.; Nah, J.; Yang, D.; Piner, R.; Velamakanni, A.; Jung, I.; Tutuc, E.; *et al.* Large-Area Synthesis of High-Quality and Uniform Graphene Films on Copper Foils. *Science* **2009**, *324*, 1312–1314.
41. Pisana, S.; Lazzeri, M.; Casiraghi, C.; Novoselov, K. S.; Geim, A. K.; Ferrari, A. C.; Mauri, F. Breakdown of the Adiabatic Born-Oppenheimer Approximation in Graphene. *Nat. Mater.* **2007**, *6*, 198–201.
42. Das, A.; Pisana, S.; Chakraborty, B.; Piscanec, S.; Saha, S. K.; Waghmare, U. V.; Novoselov, K. S.; Krishnamurthy, H. R.; Geim, A. K.; Ferrari, A. C.; *et al.* Monitoring Dopants by Raman Scattering in an Electrochemically Top-Gated Graphene Transistor. *Nat. Nanotechnol.* **2008**, *3*, 210–215.
43. Casiraghi, C. Doping Dependence of the Raman Peaks Intensity of Graphene close to the Dirac Point. *Phys. Rev. B* **2009**, *80*, 233407.
44. Kalbac, M.; Reina-Cecco, A.; Farhat, H.; Kong, J.; Kavan, L.; Dresselhaus, M. S. The Influence of Strong Electron and Hole Doping on the Raman Intensity of Chemical Vapor-Deposition Graphene. *ACS Nano* **2010**, *4*, 6055–6063.
45. Lazzeri, M.; Mauri, F. Nonadiabatic Kohn Anomaly in a Doped Graphene Monolayer. *Phys. Rev. Lett.* **2006**, *97*, 266407.
46. Yan, J.; Zhang, Y.; Kim, P.; Pinczuk, A. Electric Field Effect Tuning of Electron-Phonon Coupling in Graphene. *Phys. Rev. Lett.* **2007**, *98*, 166802.
47. Lemme, M. C.; Koppens, F. H. L.; Falk, A. L.; Rudner, M. S.; Park, H.; Levitov, L. S.; Marcus, C. M. Gate-Activated Photoresponse in a Graphene p-n Junction. *Nano Lett.* **2011**, *11*, 4134–4137.
48. Mueller, T.; Xia, F.; Avouris, P. Graphene Photodetectors for High-Speed Optical Communications. *Nat. Photonics* **2010**, *4*, 297–301.
49. Peters, E. C.; Lee, E. J. H.; Burghard, M.; Kern, K. Gate Dependent Photocurrents at a Graphene p-n Junction. *Appl. Phys. Lett.* **2010**, *97*, 193102.
50. Sun, D.; Aivazian, G.; Jones, A. M.; Ross, J. S.; Yao, W.; Cobden, D.; Xu, X. Ultrafast Hot-Carrier-Dominated Photocurrent in Graphene. *Nat. Nanotechnol.* **2012**, *7*, 114–118.
51. Graham, M. W.; Shi, S.-F.; Ralph, D. C.; Park, J.; McEuen, P. L. Photocurrent Measurements of Supercollision Cooling in Graphene. *Nat. Phys.* **2012**, *9*, 103–108.
52. Maliakal, A.; Raghavachari, K.; Katz, H.; Chandross, E.; Siegrist, T. Photochemical Stability of Pentacene and a Substituted Pentacene in Solution and in Thin Films. *Chem. Mater.* **2004**, *16*, 4980–4986.
53. Djukic, B.; Perepichka, D. F. Unexpected Formation of a Cyclic Vinylene Sulfate in the Synthesis of Ethynyl-Substituted Acenes. *Chem. Commun.* **2012**, *48*, 6651–6653.
54. Kaur, I.; Jia, W.; Kopreski, R. P.; Selvarasah, S.; Dokmeci, M. R.; Pramanik, C.; McGruer, N. E.; Miller, G. P. Substituent Effects in Pentacenes: Gaining Control over HOMO-LUMO Gaps and Photooxidative Resistances. *J. Am. Chem. Soc.* **2008**, *130*, 16274–16286.